



Cite this: DOI: 10.1039/d0nj00230e

# Temperature and magnetic dual responsive restricted access material for the extraction of malachite green from crucian and shrimp samples†

 Yuanyuan Li,<sup>id</sup>\*<sup>ab</sup> Xiangzhi Feng,<sup>id</sup><sup>ab</sup> Yulong Ma,<sup>id</sup><sup>ab</sup> Tong Chen,<sup>c</sup> Wenxin Ji,<sup>ab</sup> Xiaoxia Ma,<sup>ab</sup> Yang Chen<sup>d</sup> and Hong Xu<sup>e</sup>

A new restricted access material (RAM) based on magnetic graphene oxide (MGO) and a temperature-response polymer brush was developed and used as an adsorbent for the magnetic solid-phase extraction (MSPE) of malachite green (MG). The adsorption and desorption of MG could be achieved on the obtained smart material only through changing the temperature of the solution. At 20 °C, lower than the lower critical solution temperature (LCST) of poly (*N*-isopropylacrylamide) (PNIPAAm), the temperature-response polymer chains are swollen and are in a hydrophilic state, which can improve mass transfer and binding capacity, and further enhance recognition capability and extraction efficiency for MG. When the temperature is above the LCST, the adsorbent shows hydrophilic to hydrophobic surface property alterations, leading to a gradually weakening interaction between MG and the adsorbent material, so the captured MG molecules were released. The smart material and aqueous solution achieve separation using a magnet within 2 min. The main parameters affecting the extraction efficiency were optimized. An effective analytical method for MG was developed by combining with a UV-Vis spectrophotometer. In real sample analysis, the average recoveries with their respective relative standard deviation (RSD%) for crucian and green shrimp were 79.7–90.1 (3.8–5.3%) and 73.6–81.2 (3.7–4.3%), respectively. It indicated that the new method can be applied in the determination of MG in complex real samples.

 Received 18th January 2020,  
 Accepted 18th March 2020

DOI: 10.1039/d0nj00230e

[rsc.li/njc](http://rsc.li/njc)

## Introduction

Malachite green (MG) is a *N*-methylated diamino triphenylmethane dye, which can be used to treat bacterial infections in marine animals as an effective antibacterial and antifungal agent. It is also a dye for wool, silk, cotton, leather, *etc.*<sup>1–3</sup> As a cytotoxic chemical substance, MG has potential carcinogenic, teratogenic and mutagenic hazards for mammalian cells. MG could seriously threaten human health through channels such as the food chain and water. Therefore, researchers have paid attention to the extraction and determination of MG from living

organisms and wastewater. Although many physical and chemical treatment technologies have been developed, such as ozonation,<sup>4</sup> oxidation,<sup>5</sup> membrane filtration,<sup>6</sup> flocculation,<sup>7</sup> bio-sorption methods<sup>8</sup> and electrochemical methods,<sup>9</sup> and exhibit some interesting characteristics, some disadvantages such as slow removal process, high dissolved oxygen demand, and secondary pollution to the environment still exist.

The adsorption method based on nanomaterials is considered as a superior method for the extraction of MG, due to low cost, simplicity of operation, easy implementation and insensitivity to toxic pollutants.<sup>10</sup> Recently, graphene oxide (GO) as a nanosized carbon material, has been actively explored for use in a broad range of applications. GO has a large surface area and many hydrophilic groups such as hydroxyl, epoxide and carboxyl,<sup>11,12</sup> so it can be dispersed well in solution as an ideal adsorbent for the separation and enrichment of various compounds. However, the recovery is tedious and time-consuming for GO,<sup>13,14</sup> so magnetic nanoparticles were introduced to simplify the recycling process.<sup>15</sup> Luo *et al.* prepared a Fe<sub>3</sub>O<sub>4</sub>@SiO<sub>2</sub>@G adsorbent for the magnetic solid-phase extraction (MSPE) of sulfonamide antibiotics in water.<sup>16</sup> Lu and coworkers developed the Fe<sub>3</sub>O<sub>4</sub>@G@TiO<sub>2</sub>-based

<sup>a</sup> State Key Laboratory of High-efficiency Coal Utilization and Green Chemical Engineering, Ningxia University, Yinchuan 750021, China.

E-mail: liyuanyuan\_abc@sohu.com; Fax: +86 951 2062323; Tel: +86 951 2062330

<sup>b</sup> College of Chemistry and Chemical Engineering, Ningxia University, Yinchuan 750021, China

<sup>c</sup> Comprehensive Technology Centre, Zhenjiang Customs District, Zhenjiang, 212000, China

<sup>d</sup> Shanghe New Materials Company, Zhenjiang, 212000, China

<sup>e</sup> Zhenjiang Centre for Disease Control and Prevention, Zhenjiang 212000, China

† Electronic supplementary information (ESI) available. See DOI: 10.1039/d0nj00230e

MSPE method for the extraction and enrichment of phosphopeptides from biological samples.<sup>17</sup> Therefore, magnetic nanoparticles were loaded on graphene which not only exposes more active sites by reducing the aggregation of graphene, but also has magnetic responsiveness. It can be easily gathered using a magnetic field, and filtration, centrifugation and precipitation procedures can be omitted.<sup>18</sup> Besides, undesirable mass-transfer and binding capacity also seriously impact the accuracy of quantitative analysis in the progress of adsorption. Thus, some adsorbent materials that can improve mass transfer and binding capacity need to be prepared based on a green synthesis strategy.<sup>19–21</sup> Smart materials, particularly stimuli-responsive polymers, could reversibly change their structures and functions due to external physical, chemical or biological stimuli. It provides an alternative for improving mass transfer and binding capacity. Li *et al.* reported that a novel phycocyanin-imprinted ratiometric fluorescence nanosensor (CdTe QDs) was developed for temperature-regulated sensing and detection of a phycocyanin target.<sup>22</sup> Xiong and coworkers developed Zipper-like thermo-responsive molecularly imprinted polymers (E2-MIPs) for the selective recognition and extraction of estradiol (E2) by temperature regulation.<sup>23</sup> They can regulate the binding affinity between the target analyte and the sorbent, achieving a capture and controllable release target analyte from abundant impurities.

In our work, a poly(*N*-isopropylacrylamide) (PNIPAAm) thermo-sensitive polymer was grafted on magnetic GO (MGO) to prepare a temperature and magnetic dual responsive smart material using surface-induced ATRP technology,<sup>24</sup> which not only improves mass-transfer and binding capacity between the target analyte and the substrate, but also effectively avoids using organic solvents which can cause secondary pollution during the extraction process. PNIPAAm is a widely studied thermo-sensitive polymer. Its lower critical solution temperature (LCST) is about 32 °C.<sup>25–29</sup> It can undergo a sharp volume phase transition in aqueous solution by temperature variation around LCST.<sup>30–32</sup> For surface modification using functional polymer brushes, a “grafting-from” approach is better than a “grafting-to” approach.<sup>33,34</sup> Meanwhile, the majority of synthetic routes of ATRP use chemical coupling agents to fix the polymerization initiator onto substrates, which is environmentally unfriendly and causes secondly pollution. Inspired by mussels,<sup>35,36</sup> dopamine (DA) was applied as a bionic anchor for the polymerization of surface modification chemistry because it is non-toxic and stable. DA is a hydrophilic polymer, which can exhibit excellent dispersion in water and make effective contact between composite materials and analytes.<sup>34</sup> In addition, the  $\pi$  electrons of PDA can help absorb aromatic compounds through  $\pi$ - $\pi$  stacking interactions.<sup>37</sup> Therefore, we used PDA as a platform to anchor halogen-containing macromolecular initiators.

Compared with the existing technology, this work proposed a novel green synthesis strategy including environmental friendliness, excellent thermosensitivity, convenient separability, good mass transfer and binding capacity. Moreover, the temperature regulation system is simple, convenient and environmentally friendly.<sup>38</sup> The smart material shows a certain application potential in MSPE.

## Experimental

### Material and reagents

GO was purchased from Hunan Fenghua Material Development Co., Ltd (Hunan, China). DA hydrochloride (98%), 2,2'-bipyridine (bpy), 2-bromoisobutyrylbromide (BiBB, 98%), *N*-isopropylacrylamide (NIPAAm, 98%), MG (99%), iron(II) chloride tetrahydrate (FeCl<sub>2</sub>·4H<sub>2</sub>O) and tris(hydroxymethyl) aminoethane (Tris) were supplied by Macklin Biochemical Co., Ltd. Iron(III) chloride hexahydrate (FeCl<sub>3</sub>·6H<sub>2</sub>O), copper(I) bromide (CuBr), ammonia solution (NH<sub>3</sub>·H<sub>2</sub>O, 99.95%), *N,N*-dimethylformamide (DMF), and *cis*-oleic acid were obtained from Sinopharm Chemical Reagent Co., Ltd (Shanghai, China). Triethylamine (TEA) and *N*-hexane were purchased from Tianjin Damao Chemical Reagent Factory (Tianjin, China). NIPAAm was used after recrystallization with hexane. CuBr was purified in glacial acetic acid and then washed with ethanol. All other chemicals are of analytical grade. Deionized water (18.25 M $\Omega$ ) was obtained from a purification system (ULUPURE) throughout the experiments.

### Instruments and measurements

X-ray diffraction (XRD) patterns were recorded using a D8 Advance X-ray diffractometer. Transmission electron microscopy (TEM) images were characterized using a H-7500 TEM spectrometer (Hitachi, Japan). Thermo-gravimetric analysis (TGA) curves were conducted using a SETSYS16 Integrated Thermal Analyzer (Setaram, France). Magnetic hysteresis loops were conducted using a vibrating sample magnetometer (VSM) on a measurement system (Quantum Design, USA). X-ray photoelectron spectroscopy (XPS) spectra were obtained using an AXIS ULTRA DLD (Kratos, UK). The absorbances of MG solutions were obtained using a UV-Vis spectrophotometer (Beijing General Analysis TU-1901) at a maximum wavelength ( $\lambda_{\text{max}} = 617 \text{ nm}$ ).

### Preparation of MGO composite

MGO composite was prepared using a one-step co-precipitation method.<sup>39</sup> Briefly, GO (0.3 g) was dispersed into deionized water (50 mL) with ultrasonic treatment for 4 hours to form a uniform dispersion. Next, FeCl<sub>3</sub>·6H<sub>2</sub>O (4.0 g) and FeCl<sub>2</sub>·4H<sub>2</sub>O (2.5 g) were dissolved in deionized water and added to the above dispersion. Meanwhile, 25 mL ammonia solution was quickly added to the reaction mixture, and 0.75 mL oleic acid was injected into the mixture after stirring for 10 minutes. Then, the reaction mixture was heated using a thermostatic magnetic stirrer at 90 °C for 3 h. After that, MGO was washed several times with deionized water and ethanol. The product was collected by magnetic separation and dried under vacuum at 70 °C overnight.

### Preparation of polydopamine-coated MGO based on ATRP initiator

ATRP initiator (DA-BiBB) was prepared using Edmondson's method.<sup>40</sup> BiBB and DA could copolymerize into a PDA film containing ATRP-initiating groups. Briefly, DA (400 mg, 2.10 mmol) was dissolved in DMF (10 mL) and was degassed by purging with dry N<sub>2</sub> for 10 min. BiBB (2.10 mmol) and TEA

(2.10 mmol) were added dropwise to the solution and reacted for 30 minutes at 0 °C. The ice-water bath was removed, and the reaction occurred for 3 h under a N<sub>2</sub> atmosphere at room temperature. Then, this mixture was transferred to a glass beaker (500 mL). Tris (480 mg, 4.0 mmol), MGO (0.15 g) and deionized water (100 mL) were added to the mixture, and stirred for 24 h at room temperature. The obtained product (MGO@PDA-Br) was washed several times with deionized water and ethanol and separated by magnetic separation, then dried under vacuum at 60 °C overnight for further use.

### Synthesis of PNIPAAM grafted MGO (MGO@PDA@PNIPAAM)

100 mg MGO@PDA-Br was dispersed in methanol/water (v/v, 10/10) by ultrasonication in a dry Schlenk flask. NIPAAM (2.0 g), CuBr (0.12 g), and bpy (0.36 g) were added to the mixture under a N<sub>2</sub> atmosphere, followed by further bubbling with N<sub>2</sub> for 30 minutes. Then, polymerization was performed for 24 h at 60 °C under a N<sub>2</sub> atmosphere. The final product MGO@PDA@PNIPAAM was collected with a magnet, intensively washed with ethanol and water respectively, and then dried under vacuum at 40 °C for 12 h. The synthesis process is shown in Scheme 1.

### Batch adsorption experiments

Equilibrium data is important to obtain more insight into adsorption and bonding properties between the target molecules and the adsorbent.<sup>41</sup> It also helps to understand the mechanisms in the adsorption process. In this work, some parameters were optimized. Besides, Langmuir, Freundlich isotherms, pseudo-first-order and pseudo-second-order kinetics were used to investigate the adsorption mechanism of MG on the adsorbent material.

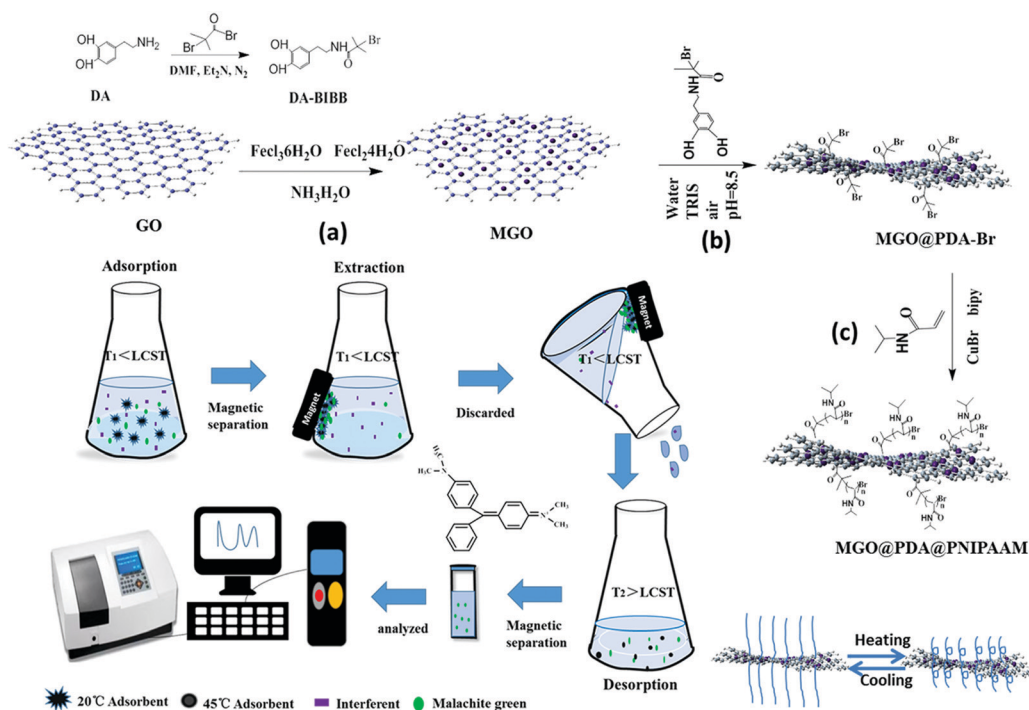
In a batch process, 5 mg of the adsorbent was added to a 50 mL conical flask, and 10 mL of MG solution was accurately measured with a pipette and added into the conical flask. All the adsorption experiments were performed in a thermo-static oscillator at 20 °C with 150 rpm. After the equilibrium point, the conical flasks were taken out and separation was achieved between the MG solution and the adsorbent material within 2 minutes by a magnet, and the solution was filtered with a 0.22 μm PTFE syringe filter. The absorbances of MG ( $\lambda_{\text{max}} = 617 \text{ nm}$ ) before and after adsorption were measured using a UV-Vis spectrophotometer in each adsorption experiment. Then, the MG concentration was calculated according to the standard working curve (Table S1 and Fig. S1, ESI†).

### Optimization of variables

Various parameters were optimized, such as MG concentration (0.1–35 μg mL<sup>-1</sup>), contact time (10–180 min), pH (3–10) and ionic strength (0.02–0.1 M). By changing the initial concentration of MG, the effect on adsorption capacity was investigated under constant conditions of pH, dosage of adsorbent and ambient temperature (20 °C). Then, the effect of contact time was investigated. In each series of experiments, the samples were tested at specified intervals (10–180 min). Subsequently, the effect of pH (3–10) value was studied at the optimal concentration and time. Finally, the effect of ionic strength was researched at a NaCl concentration of 0.02–0.1 M. The adsorption capacity was evaluated by the following equation:

$$q_e = \frac{(C_o - C_e)m}{V}$$

where,  $q_e$  (mg g<sup>-1</sup>) is the adsorption quantity;  $C_o$  (μg mL<sup>-1</sup>) and  $C_e$  (μg mL<sup>-1</sup>) are the initial and equilibrium concentration of MG;



Scheme 1 The synthesis and adsorption process of MGO@PDA@PNIPAAM.

$V$  (mL) is the volume of MG solution;  $m$  (mg) is the amount of MGO@PDA@PNIPAAM. All the adsorption experiments were performed at least in triplicate for data analysis.

### Desorption and regeneration

After the extraction procedure was performed under optimal conditions, the sorbent and MG solution were quickly separated by an external magnetic field force and the solution was then discarded. Then, the target analyte was eluted with water (without additional chemicals) at 45 °C. Reasons for the selection of temperature can be attributed to the temperature-responsive behavior of MGO@PDA@PNIPAAM by a temperature variation around 32 °C. The adsorbent material was reused for 5 cycles to assess the recyclability.

### Sample preparation

A stock MG solution was prepared at a concentration of 1.0 mg mL<sup>-1</sup>, using fresh ultrapure water in a tight and light-resistant volumetric flask and stored in a freezer at 4 °C. MG is stable in the temperature range studied. MG standard solution at a concentration of 100 µg mL<sup>-1</sup> was prepared by diluting stock standard solution with ultrapure water. Then, it was diluted with different volumes of ultrapure water to prepare the working solutions with various concentrations of 0.1–35 µg mL<sup>-1</sup> for the subsequent experiments. In all experiments, the stock solution can be stored in a freezer at 4 °C for one month. Other standard working solutions need to be reconstituted at each use.

Crucian and green shrimp samples were obtained from a local market. Before extraction, the crucian tissue was separated from bones and skin, and the shrimp shell and line were removed from the shrimp. They were ground into a homogenate using a mortar. 25 g of two samples and 20 mL of acetonitrile were transferred to a 50 mL centrifuge tube, and were sonicated for 15 minutes, respectively. They were centrifuged at 8000 rpm for 5 minutes and the supernatants were collected. This process was repeated three times. Then, all the extraction solutions were merged, and concentrated *via* a rotary evaporator at 50 °C. The residues on the wall of the bottle were washed with 1 mL of acetonitrile 3 times and were then concentrated further. They were filtered through a 0.22 µm PTFE syringe filter and transferred to volumetric flasks, which were diluted to a final volume of 50 mL with ultrapure water. They were stored at 4 °C and used in the MSPE procedure.

## Results and discussion

### Characterization of MGO@PDA@PNIPAAM

The synthesized composite was characterized using different techniques. A TGA technique was used to determine the degree of organic functionalization. Fig. 1 shows the TGA curves of MGO, MGO@PDA-Br, and MGO@PDA@PNIPAAM. The weight loss of MGO (Fig. 1a) was about 20.15% from 25 °C to 800 °C, which was attributed to the evaporation of water molecules, removal of oxygen-containing functional groups and the decomposition of carbon skeleton.<sup>42</sup> Compared with it, MGO@PDA-Br

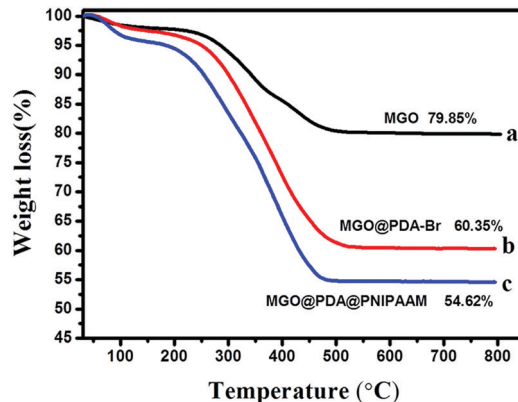


Fig. 1 TGA curves of MGO (a), MGO@PDA-Br (b), MGO@PDA@PNIPAAM (c).

(Fig. 1b) demonstrated a weight loss of approximately 39.65% with the same temperature range due to the loss of PDA-Br. When NIPAAM was grafted on to MGO@PDA-Br *via* ATRP technology, the weight loss was around 45.38%, owing to the decomposition of PNIPAAM (Fig. 1c).

The magnetic properties of the functional GO were studied by VSM. Fig. 2 shows the magnetic hysteresis loops of MGO, MGO@PDA-Br, and MGO@PDA@PNIPAAM. They indicate that all functionalized GO have superparamagnetic properties. Their magnetization saturation ( $M_s$ ) values are 52.97, 38.87 and 32.66 emu g<sup>-1</sup>, respectively. MGO was covered by organic substances including PDA-Br and PNIPAAM, which caused the  $M_s$  value reduction. However, it still exhibits excellent magnetic responsiveness. For example, MGO@PDA@PNIPAAM can be completely separated from MG solution by an external magnetic field within 2 minutes (Fig. 2, inset). Furthermore, MGO@PDA-Br and MGO@PDA@PNIPAAM were investigated *via* incubating dispersions using a constant-temperature water bath at 20 °C and 45 °C. When the temperature of the solution is below the LCST, the PNIPAAM chains are swollen in water, which dispersed homogeneously in water (Fig. 3A-b). When the temperature is higher than the LCST, they become shrunken and are precipitated

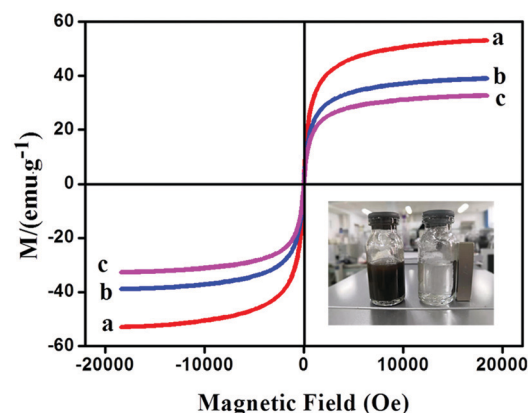


Fig. 2 The magnetic hysteresis loops of MGO (a), MGO@PDA-Br (b), and MGO@PDA@PNIPAAM (c). The optical image of MG solution with MGO@PDA@PNIPAAM: left inset (without an external magnetic field), right inset (with an external magnetic field).

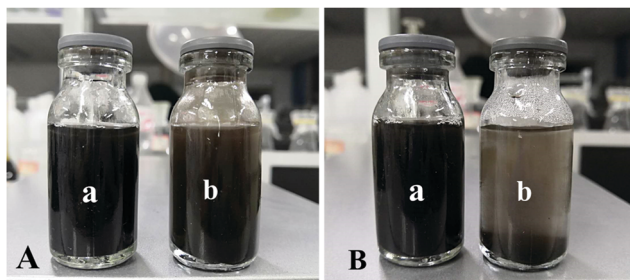


Fig. 3 The optical images of MGO@PDA-Br (a) and MGO@PDA@PNIPAAm (b) dispersion in water at 20 °C (A) and 45 °C (B).

out from the water (Fig. 3B-b). It is indicated that MGO@PDA@PNIPAAm has excellent thermosensitivity in water around LCST. However, MGO@PDA-Br was evenly dispersed at 20 °C or 45 °C, which suggested that it remained without thermosensitivity. Therefore, both typical temperatures of 20 °C and 45 °C were studied. Meanwhile, it also provided evidence that PNIPAAm chains were successfully immobilized on the surfaces of MGO.

The TEM images are shown in Fig. 4. Firstly, Fig. 4a presents the TEM image of GO, which has a large number of adsorption sites. As can be seen, Fig. 4b reveals a different surface with many particles (size around 10 nm) due to the presence of Fe<sub>3</sub>O<sub>4</sub> nanoparticles on the GO surface, which demonstrated that GO had been successfully modified by Fe<sub>3</sub>O<sub>4</sub> nanoparticles and endowed the GO nanocomposite with excellent magnetic separability. As shown in Fig. 4c, a thin coating can be clearly observed compared with MGO, which was attributed to the fact that a PDA-Br layer was formed when BiBB-DA was anchored onto the MGO.<sup>43</sup> After PNIPAAm was grafted onto MGO@PDA-Br, its TEM image (Fig. 4d) shows some furry structures compared with the former. It could be observed that there were a lot of curled and tangled brushes evenly decorated on the MGO sheet, which can imply the successful preparation of MGO@PDA@PNIPAAm.

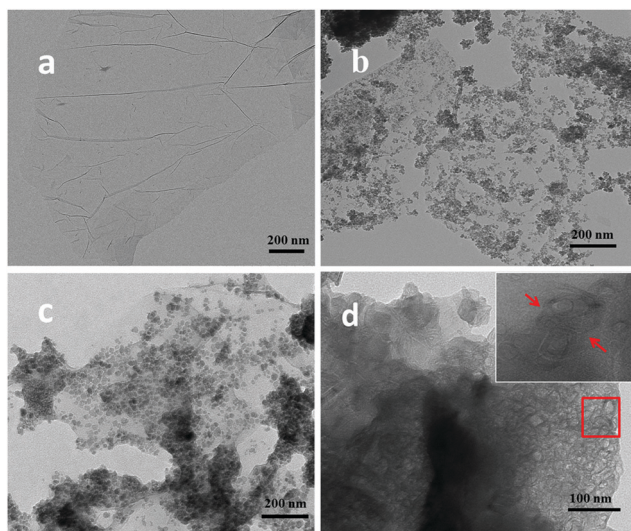


Fig. 4 TEM images of GO (a), MGO (b), MGO@PDA-Br (c), and MGO@PDA@PNIPAAm (d).

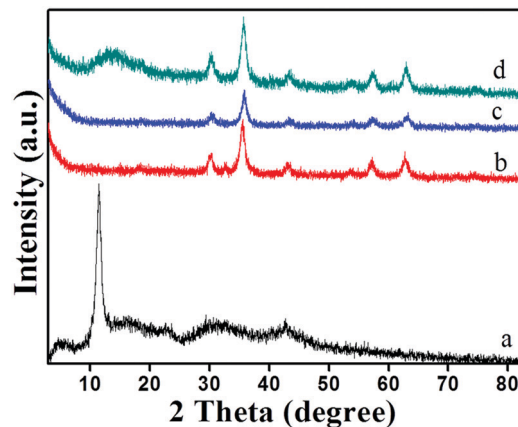


Fig. 5 XRD pattern of GO (a), MGO (b), MGO@PDA-Br (c), and MGO@PDA@PNIPAAm (d).

XRD was used to characterize the crystalline structures of GO (a), MGO (b), MGO@PDA-Br (c), and MGO@PDA@PNIPAAm (d). The results are shown in Fig. 5. The peak of GO located at  $2\theta \approx 11^\circ$ , which was consistent with the reported results.<sup>44</sup> The spectrum of MGO includes six characteristic diffraction peaks at  $30.32^\circ$ ,  $36.56^\circ$ ,  $43.36^\circ$ ,  $53.76^\circ$ ,  $57.20^\circ$  and  $63.96^\circ$ . These peaks are characteristic of Fe<sub>3</sub>O<sub>4</sub>. Therefore, it can be inferred that there was a considerable connection between GO and Fe<sub>3</sub>O<sub>4</sub>, retaining the crystal structure of Fe<sub>3</sub>O<sub>4</sub> and ensuring the magnetic property of the composite material. As shown in Fig. 5c, the result revealed that the PDA film introduced on the surface of MGO did not change the crystal structure, and MGO@PDA-Br still had a typical cubic spinel structure. As shown in Fig. 5d, there was a specific broad peak at  $2\theta \approx 15^\circ$  after PNIPAAm was bonded, which indicated that the polymer was successfully grafted on MGO@PDA-Br.

Fig. 6 displays the XPS spectra of MGO (a), MGO@PDA-Br (b) and MGO@PDA@PNIPAAm (c). They confirm that the initiator was immobilized and PNIPAAm was successfully grafted on GO by analyzing the surface chemical compositions of those nanocomposites. As shown in Fig. 6a, the appearance of the Fe 2p

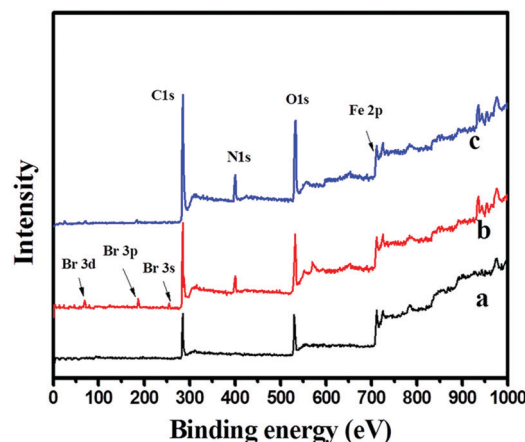


Fig. 6 XPS spectra of MGO (a), MGO@PDA-Br (b), and MGO@PDA@PNIPAAm (c).

peak component at the binding energy around 709.96 eV in the wide scan spectrum of MGO, indicated that  $\text{Fe}_3\text{O}_4$  particles were successful immobilized on GO. In the wide scan spectrum of MGO@PDA-Br (Fig. 6b), the N 1s peak at 399.64 eV, the Br 3d peak, Br 3p peak and Br 3s peak at 69.99 eV, 182.25 eV and 255.35 eV appeared, respectively. It confirmed that MGO was modified with PDA layers, bearing the ATRP initiator. In addition, the increase of C 1s, N 1s and O 1s and the disappearance of the Br peak in Fig. 6c were observed. They indicated that PNIPAAm was successfully grafted onto the MGO@PDA-Br.

### Optimization of the enrichment conditions for MG

**Adsorption isotherms.** The MGO@PDA@PNIPAAm smart material shows a temperature responsive adsorption performance in low/high temperature processes. To investigate the maximum adsorption capacity of the smart material, a constant dosage (5 mg) of MGO@PDA@PNIPAAm and different concentrations of MG ( $0.1\text{--}35\ \mu\text{g mL}^{-1}$ ) were used for MSPE. After adsorption equilibrium, the absorbances of MG solution were measured using a UV-Vis spectrophotometer. As shown in Fig. 7, the maximum adsorption capacity was obtained when the concentration was  $30\ \mu\text{g mL}^{-1}$  at  $20\ ^\circ\text{C}$  and  $20\ \mu\text{g mL}^{-1}$  at  $45\ ^\circ\text{C}$ . This is because the material shows a hydrophilic property at  $20\ ^\circ\text{C}$ , so that more hydrophilic MG molecules can be adsorbed. As the temperature increased from  $20\ ^\circ\text{C}$  to  $45\ ^\circ\text{C}$ , the PNIPAAm chains changed from a swollen state to a shrunken and hydrophobic state, which resulted in the hydrophobic property of the material. Therefore, the interaction weakens between the smart material and MG, and causes desorption of the captured MG molecules from the adsorbent.

Two parameter isotherm models of Langmuir and Freundlich were used to obtain the best of the equilibrium curves. Langmuir isotherm (eqn (1)) assumes homogeneous adsorption and adsorption only occurring at specific homogeneous sites. Freundlich isotherm (eqn (2)) is an empirical model which describes multi-layer adsorption.

$$\frac{C_e}{q_e} = \frac{1}{q_{\max}K_L} + \left(\frac{1}{q_{\max}}\right)C_e \quad (1)$$

$$\ln q_e = \ln K_F + \frac{\ln C_e}{n} \quad (2)$$

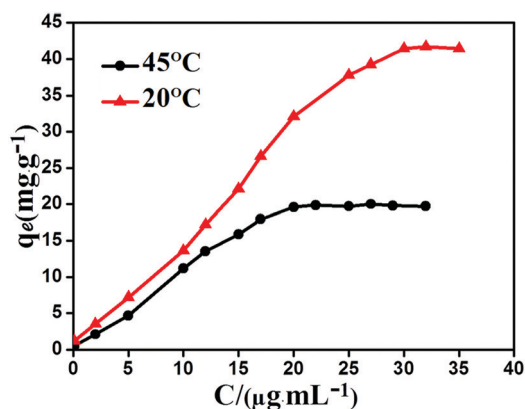


Fig. 7 Adsorption isotherms of MG on the smart material.

where  $q_e$  ( $\text{mg g}^{-1}$ ) is the adsorption capacity,  $C_e$  ( $\mu\text{g mL}^{-1}$ ) is the equilibrium concentration in water,  $q_{\max}$  ( $\text{mg g}^{-1}$ ) is the theoretical saturate adsorption capacity in the Langmuir model, and  $K_L$  ( $\text{mL } \mu\text{g}^{-1}$ ) is the Langmuir isotherm constant demonstrating the tendency of adsorption,  $K_F$  is the Freundlich isotherm constant and  $n$  is the heterogeneity factor.

As shown in Fig. 8, the two isotherm adsorption models ( $20\ ^\circ\text{C}$  and  $45\ ^\circ\text{C}$ ) were linearly fitted, and the calculated model constants and statistical parameters are summarized in Table 1.  $R^2$  values show a strong linear relationship between the predicted and experimental Langmuir model values, which indicate a monolayer adsorption of MG onto the MGO@PDA@PNIPAAm. Lower  $R^2$  values of the Freundlich isotherm model confirm that experimental data does not agree well with the Freundlich isotherm.

**Adsorption kinetics.** To understand the adsorption mechanisms and the influence of adsorption time, kinetic experiments were performed at  $20\ ^\circ\text{C}$  and  $45\ ^\circ\text{C}$ . 5 mg adsorbent and concentrations ( $30\ \mu\text{g mL}^{-1}$  at  $20\ ^\circ\text{C}$  and  $20\ \mu\text{g mL}^{-1}$  at  $45\ ^\circ\text{C}$ ) of MG were constant, and the contact time was investigated from 10 to 180 minutes during the MSPE process. As shown in Fig. 9, the adsorption processes were very quick before 30 minutes, which might be attributed to a large number of binding sites on the surfaces of MGO@PDA@PNIPAAm and collisional probability between MG and the sorbent. As time increased to 90 minutes, the adsorption equilibrium could be achieved, which could be attributed to the saturation of active sites on surfaces of the smart material. They need 90 minutes to reach equilibrium at different temperatures ( $20\ ^\circ\text{C}$  or  $45\ ^\circ\text{C}$ ), which were mainly ascribed to the fact that MG may need more time through the layer of collapsed PNIPAAm chains to reach the surface of the MGO sheet.

The pseudo-first order model (eqn (3)) assumes that the sorption rate decreases linearly with the increase of adsorption capacity. The pseudo-second order kinetics model (eqn (4)) assumes that the rate-limiting step is the interaction between the two reagent particles, which is used to describe a chemical adsorption.

$$\ln(q_e - q_t) = \ln q_e - k_1 t \quad (3)$$

$$\frac{t}{q_t} = \frac{1}{k_2 q_e^2} + \frac{t}{q_e} \quad (4)$$

Where  $q_e$  and  $q_t$  ( $\text{mg g}^{-1}$ ) are the amounts of analyte on the adsorbents at equilibrium and time  $t$  (min).  $k_1$  ( $\text{min}^{-1}$ ) is the rate constant in the pseudo-first order adsorption model and  $k_2$   $\text{g}(\text{mg min})^{-1}$  is the rate constant in the pseudo-second order adsorption model.

As shown in Fig. 10, the obtained experimental data were fitted to different kinds of kinetic models about pseudo-first order and pseudo-second order. The fitting results of kinetic data and statistical parameters are listed in Table 2. According to the results shown,  $R^2$  of the pseudo-second-order kinetic model was higher than the pseudo-first-order kinetic model and the value of  $q_{e,\text{cal}}$  was also close to the experimental value of  $q_{e,\text{exp}}$ . It indicated that the adsorption could be well described by

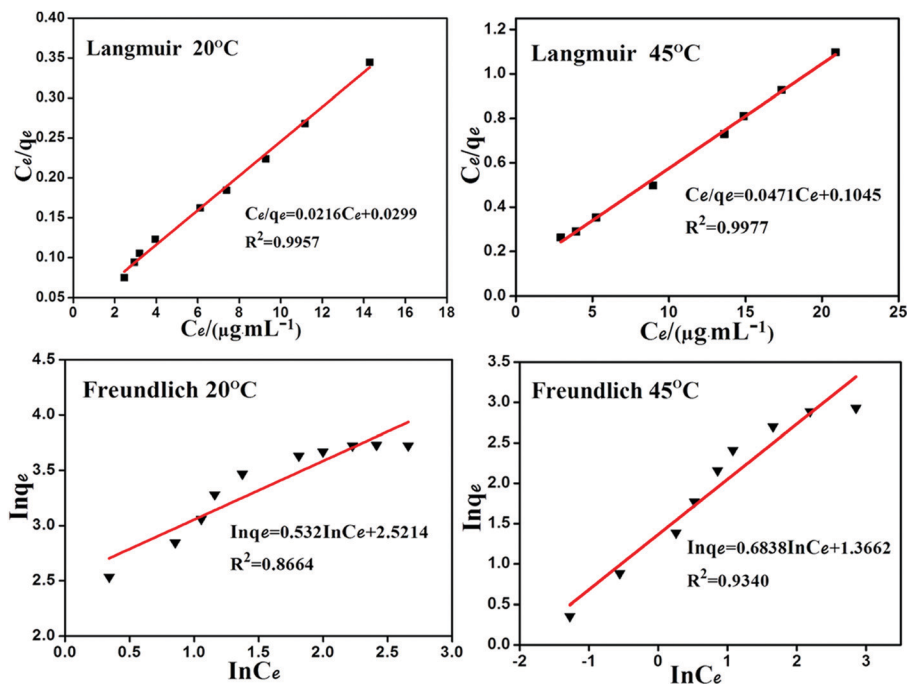


Fig. 8 The linear fit of the Langmuir isotherm and Freundlich isotherm at 20 °C and 45 °C.

Table 1 Isothermal parameters for the adsorption of MG onto the smart material

Contaminant	Temperature (°C)	Langmuir model			Freundlich model		
		$q_{\max}$ (mg g <sup>-1</sup> )	$K_L$ (L mg <sup>-1</sup> )	$R^2$	$K_F$ (mg <sup>1-n</sup> L <sup>n</sup> g <sup>-1</sup> )	$n$	$R^2$
	20	46.2961	0.7224	0.9957	12.4460	1.8797	0.8664
	45	21.2314	0.4507	0.9977	3.9204	1.4624	0.9340

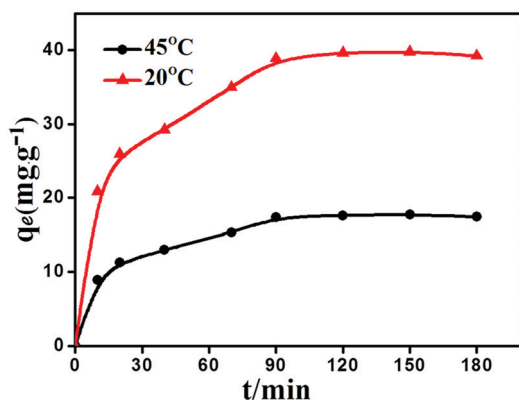


Fig. 9 Adsorption kinetics of MG on the smart material.

the pseudo-second-order mechanism and the experimental process was mainly based on the chemical adsorption.

### Effect of solution pH on adsorption efficiency

The pH value of the solution has an important influence during the MSPE process, because the structure of MG and surface

property of the adsorbent changed with pH. The green-blue color of MG remains unaffected at acidic and neutral pH, but under the condition of alkaline pH, could cause a change of the structure and stability. In this work, the effect of solution pH on adsorption efficiency was investigated by adjusting the pH from 3 to 10 at two different temperatures (20 °C and 45 °C). Meanwhile, the characteristics of the smart material were further explained by comparing with MGO.

As shown in Fig. 11, a lower pH (pH < 7.0) was not conducive to the progress of adsorption, a possible reason for this could be attributed to the fact that excess H<sup>+</sup> ions compete with the positively charged MG molecules to reach the adsorbent surfaces when pH < 7, so the adsorption capacity was greatly reduced. When pH = 7, the  $q_e$  always reached the largest value ( $q_{e,\max}$ ) for each adsorbent. The concentration of H<sup>+</sup> could be neglected, so the competition between H<sup>+</sup> and MG molecules was also negligible. It is worth noting that the color of the MG solution became gradually lighter or disappeared due to the change of the structure of MG molecule when pH > 9.0. Thus, it is beneficial for practical applications without pH adjustment. As shown in Fig. 11, the adsorption capacity of

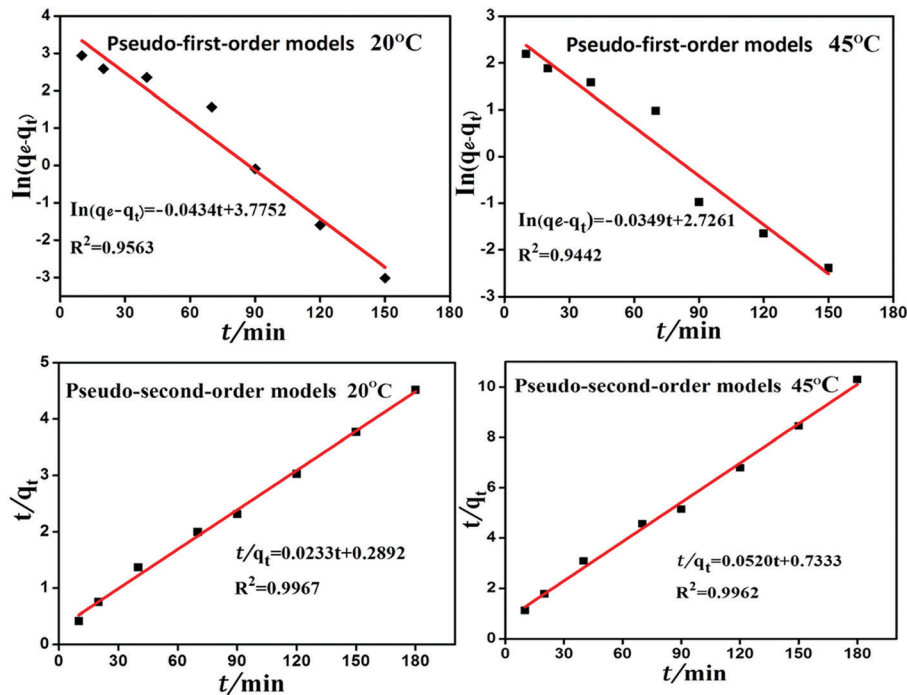
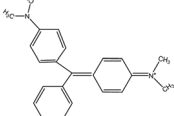


Fig. 10 The linear fit of pseudo-first-order kinetic model and pseudo-second-order kinetic model at 20 °C and 45 °C.

Table 2 Kinetic parameters for the adsorption of MG onto the smart material

Contaminant	Temperature (°C)	Pseudo-first order			Pseudo-second order		
		$q_{e1}$ (mg g <sup>-1</sup> )	$K_1$ (min <sup>-1</sup> )	$R^2$	$q_{e2}$ (mg g <sup>-1</sup> )	$K_2$ (g (mg <sup>-1</sup> min <sup>-1</sup> ))	$R^2$
	20	43.6062	0.0434	0.9563	42.9185	0.0019	0.9967
	45	15.2732	0.0349	0.9442	19.2308	0.0037	0.9962

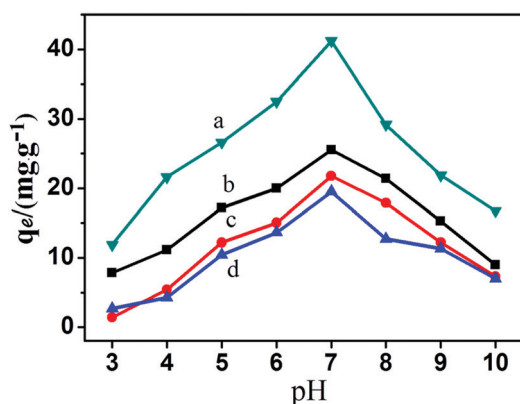


Fig. 11 Effect of pH on the adsorption of MG onto MGO@PDA@PNIPAAM at 20 °C (a) and 45 °C (d), and onto MGO at 45 °C (b) and 20 °C (c).

MGO slightly increased when the temperature changed from 20 °C to 45 °C. Compared with MGO, the smart material adsorption behavior was completely opposite. Therefore, it is

indicated that MGO@PDA@PNIPAAM has a temperature-responsive adsorption behavior. The adsorption amount of MGO@PDA@PNIPAAM attain  $Q_{e,max} = 41 \text{ mg g}^{-1}$  at 20 °C. Although PNIPAAM grafted onto the MGO sheet may cover partial surfaces of MGO@PDA@PNIPAAM, the  $\pi$  electrons of PDA can help it to absorb MG *via*  $\pi$ - $\pi$  stacking interactions.<sup>31</sup> Moreover, the hydrophilic smart material shows excellent dispersibility in solution and promotes an effective contact between the composite and the target analyte. In the case of 45 °C, the adsorption capacity of MGO@PDA@PNIPAAM was slumped to  $19 \text{ mg g}^{-1}$ . The reason for this might be that the whole PNIPAAM chains were changed from a swollen state to a shrunken one, leading to the interaction gradually weakening between MG and the adsorbent material, so the captured MG molecules were released. In the meantime, it is also directly proved that the grafted PNIPAAM brushes play a key role in MSPE. Besides, another hint was obtained from the temperature-responsive adsorption behavior that a change of temperature could promote the regeneration of the hydrophilic adsorbent when it was higher than the LCST of NIPAAM.

### Effect of ionic strength on adsorption efficiency

The effect of ionic strength on adsorption efficiency was studied in the coexistence of NaCl. The salt ionic concentration has a significant effect on the adsorption capacity when the temperature is at 20 °C and 45 °C. As the concentration of NaCl increased from 0.02 to 0.1 M in Fig. 12, the adsorption capacity of the smart material decreased. A possible reason for this could be attributed to the fact that  $\text{Na}^+$  competed with MG molecules in the solution, and occupied the active sites on the surfaces of the adsorbent during the adsorption process, so the adsorption capacity of the smart material was weakened for MG. It was also indirectly proved that there exist an electrostatic interaction between MG and the adsorbent during the MSPE process. Additionally, the hydrogen bond and  $\pi$ - $\pi$  stacking interaction might also influence the adsorption in the extraction process. Possible mechanisms for this are shown in Scheme 1.

### Desorption and regeneration

The regeneration performance of MGO@PDA@PNIPAAM was assessed. The desorption experiment was carried out using a thermostatic oscillator at 45 °C, and the material was regenerated by changing the water temperature without other additional chemicals. During the desorption process, the smart material was eluted with 3 mL hot water at each time point, and repeatedly until maximum recovery was obtained. The effect of eluent volume accumulated was evaluated using 3, 6, 9, 12 and 15 mL hot water. The results are shown in Fig. 13(a) and 12 mL was

selected as the eluent volume accumulated. After desorption, the collected MGO@PDA@PNIPAAM material was washed alternately with hot/cold water several times, and then dried in vacuum at 60 °C overnight for the next cycle.

During the reusing process, the number of cycles is an important parameter for obtaining good recoveries. The results showed that MGO@PDA@PNIPAAM could be reused at least 5 times without a significant loss of adsorbent capacity as shown in Fig. 13(b). The adsorption capacity of MG was still above 36  $\text{mg g}^{-1}$  after five cycles of use. Therefore, MGO@PDA@PNIPAAM has good reusability.

### Method validation

The proposed method was evaluated by several parameters such as the linearity, limits of detection (LOD), recovery, reuse and precision. The concentration of calibration curve ranged from 0.1–35  $\mu\text{g mL}^{-1}$ , the linearity was  $A = 0.1907C - 0.1121$  and the correlation coefficient ( $R^2$ ) was 0.9987. Good linearity was obtained in the studied concentration range. The enrichment factor (EF) was 83 and the limit of detection (LOD) was 0.08  $\mu\text{g mL}^{-1}$ . The accuracy of the method was evaluated by recovery tests. The precision of the method was evaluated by repeatability (intraday) and reproducibility (interday) studies, performed by spiking known quantities of the standard solution (different concentrations of 10, 20 and 30  $\mu\text{g mL}^{-1}$ ) to known amounts of real samples. The resultant samples were analyzed using this method, and the results are shown in Table 3. Accordingly, a good correlation exhibits the effective

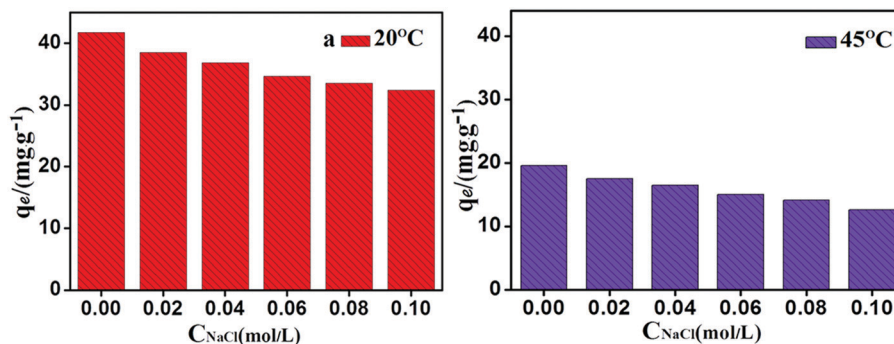


Fig. 12 Effect of ionic strength.

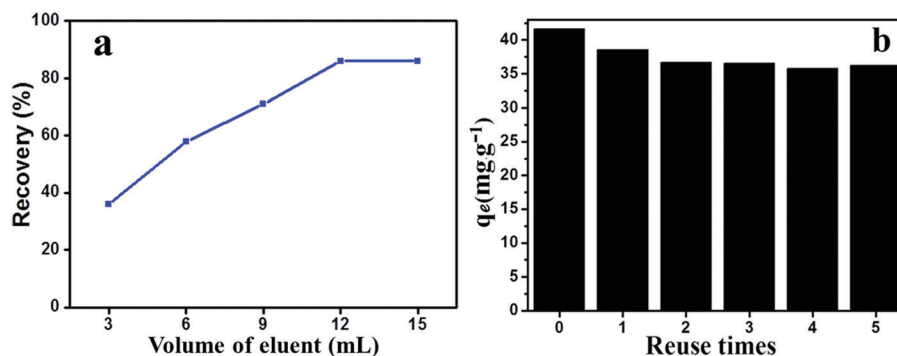


Fig. 13 The volume of eluent (a), and the adsorption capacity after five cycles of reuse (b).

**Table 3** The recovery results of MG at three different spiking levels in real samples and intra-day and inter-day precisions

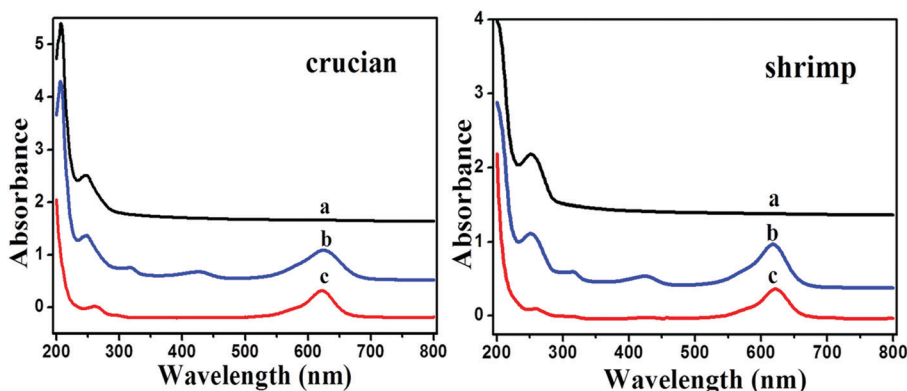
Real sample	Spike level ( $\mu\text{g mL}^{-1}$ )	Recovery (%)	RSD (%), $n = 3$	Intra-day precision (RSD, %, $n = 6$ )	Inter-day precision (RSD, %, $n = 3$ )
Green shrimp	0	ND	—	—	—
	10	76.5	3.7	4.2	5.3
	20	81.2	4.3	5.6	4.7
	30	73.6	3.9	3.5	6.1
Crucian	0	ND	—	—	—
	10	82.4	5.3	3.7	4.6
	20	79.7	3.8	4.3	3.9
	30	90.1	4.7	5.7	6.5

performance of the proposed method for the extraction of MG in complex environmental samples.

### Analysis of real samples

To validate the applicability and reliability of the smart material, it was used as a sorbent for pre-concentration and determination of MG in real samples. The preprocessed samples of crucian and green shrimp were spiked with MG concentrations of  $10 \mu\text{g mL}^{-1}$ ,  $20 \mu\text{g mL}^{-1}$  and  $30 \mu\text{g mL}^{-1}$ , respectively. The recoveries of MG were evaluated in real samples under optimized conditions using the developed method. The results are listed in Table 3. It showed that MG was not detected in un-spiked real samples. In the spiked samples, the recoveries ranged from 79.7 to 90.1% for crucian and 73.6 to 81.2% for green shrimp, which indicated that the developed method is suitable for the pre-concentration and determination of MG in real samples.

Fig. 14 shows the spectrum of the unspiked real sample (a), the spiked real sample with  $3 \mu\text{g mL}^{-1}$  (b), and the eluted spectrum (c). It indicates that the smart material could concentrate and enrich MG.

**Fig. 14** Typical spectrum of the unspiked real sample (a), the spiked real sample (b), and the eluted spectrum (c).**Table 4** Comparison of the proposed method with other methods applied for MG

Adsorbent	Analysis technique	Dosage of sorbent (mg)	Linear range	Regeneration method	Ref.
MBCNF/GOPA	UV-Vis	5	$5\text{--}50 \text{ g mL}^{-1}$	Acetic acid/methanol	45
$\text{Fe}_3\text{O}_4$ @Mel	UV-Vis	300	$0.1\text{--}8 \text{ g mL}^{-1}$	Acetic acid	46
MMIPs	HPLC-UV	10	$2\text{--}1000 \text{ ng mL}^{-1}$	Methanol/acetic acid	47
$\text{Fe}_3\text{O}_4$ @PEI-MOF-5	UHPLC-MS/MS	10	$1\text{--}500 \text{ ng mL}^{-1}$	Methanol/formic acid	48
MGO@PDA@PNIPAAM	UV-Vis	5	$0.1\text{--}35 \text{ g mL}^{-1}$	Hot/cold water	This work

### Comparison with other methods

The analytical results obtained using the proposed method are compared with those used in the literature for analyzing MG. The methods were compared by evaluating the parameters including analysis technique, dosage of sorbent, linear range and regeneration method. The results are presented in Table 4. The proposed method mainly exhibits lower amounts of the sorbent and a wide linear range. The material was eluted and regenerated in alternatively hot/cold water without an organic solvent. It suggested that the proposed method was much simpler and environmentally friendly because the consumption of solvent decreased.

### Conclusions

A temperature and magnetic dual responsive restricted access material MGO@PDA@PNIPAAM was prepared, characterized and evaluated. The material as an adsorbent could accomplish adsorption and desorption of MG only by changing the temperature of the aqueous solution without other additional chemicals. Compared with the previous reported methods<sup>45–48</sup> using an organic solvent as an eluent, the new method does not cause secondary environmental pollution. At the same time, the smart material could be quickly and completely separated from the aqueous solution by magnets within 2 minutes in the recycling process, which greatly saves time and simplifies the cumbersome separation process. An effective enrichment method for MG was developed and successfully applied to the analysis of MG in real samples with satisfactory recoveries. The material and the developed method will be convenient, reliable and promising for the determination of MG in complex samples.

## Conflicts of interest

There are no conflicts to declare.

## Acknowledgements

This work was supported by the Research Project for Science and Technology of Higher Education of Ningxia Province of China (NGY 2018014), the Ningxia Natural Science Foundation of China (2019AAC03023), the East-West Cooperation Project of Ningxia Key R&D Plan (2017BY064,2019BFH02014), the Zhenjiang Social Development Project (SH2018017) and the National First-rate Discipline Construction Project of Ningxia (NXYLXK2017A04).

## References

- 1 A. Mohamed, M. M. Ghobara, M. K. Abdelmaksoud and G. G. Mohamed, *Sep. Purif. Technol.*, 2019, **210**, 935–942.
- 2 C. Pradeep Sekhar, S. Kalidhasan, N. Rajesh and V. Rajesh, *Chem*, 2009, **77**, 842–847.
- 3 W. Qu, T. Yuan, G. Yin, S. Xu, Q. Zhang and H. Su, *Fuel*, 2019, **249**, 45–53.
- 4 E. Kusvuran, O. Gulnaz, A. Samil and Ö. Yildirim, *J. Hazard. Mater.*, 2011, **186**, 133–143.
- 5 M. S. Sajab, C. H. Chia, C. H. Chan, S. Zakaria, H. Kaco, S. W. Chook, S. X. Chin and A. A. M. Noor, *RSC Adv.*, 2016, **6**, 19819–19825.
- 6 S. M. Doke and G. D. Yadav, *Chem*, 2014, **117**, 760–765.
- 7 H. Wu, R. Yang, R. Li, C. Long, H. Yang and A. Li, *Environ. Sci. Pollut. Res.*, 2015, **22**, 13038–13048.
- 8 W. Tsai and H. Chen, *J. Hazard. Mater.*, 2010, **175**, 844–849.
- 9 F. Guenfoud, M. Mokhtari and H. Akrouf, *DiamRelater*, 2014, **46**, 8–14.
- 10 Y. Dai, N. Zhang, C. Xing, Q. Cui and Q. Sun, *Chem*, 2019, **223**, 12–27.
- 11 H. He and C. Gao, *ACS Appl. Mater. Interfaces*, 2010, **2**, 3201–3210.
- 12 P. Sharma and M. R. Das, *J. Chem. Eng. Data*, 2012, **58**, 151–158.
- 13 H. C. Schniepp, J. Li, M. J. McAllister, H. Sai, M. Herrera-Alonso, D. H. Adamson, R. K. Prud'Homme, R. Car, D. A. Saville and I. A. Aksay, *J. Phys. Chem. B*, 2006, **110**, 8535–8539.
- 14 Z. Wang, J. Zhang, P. Chen, X. Zhou, Y. Yang, S. Wu, L. Niu, Y. Han, L. Wang, P. Chen, F. Boey, Q. Zhang, B. Liedberg and H. Zhang, *Biosens. Bioelectron.*, 2011, **26**, 3881–3886.
- 15 Y. Ma, Y. Li, G. Zhao, L. Yang, J. Wang, X. Shan and X. Yan, *Carbon*, 2012, **50**, 2976–2986.
- 16 Y. Luo, Z. Shi, Q. Gao and Y. Feng, *J. Chromatogr. A*, 2011, **1218**, 1353–1358.
- 17 J. Lu, C. Deng, X. Zhang and P. Yang, *ACS Appl. Mater. Interfaces*, 2013, **5**, 7330–7334.
- 18 X. Li, G. Zhu, Y. Luo, B. Yuan and Y. Feng, *TrAC, Trends Anal. Chem.*, 2013, **45**, 233–247.
- 19 A. Ostovan, M. Ghaedi, M. Arabi, Q. Yang, J. Li and L. Chen, *ACS Appl. Mater. Interfaces*, 2018, **10**, 4140–4150.
- 20 A. R. Bagheri, M. Arabi, M. Ghaedi, A. Ostovan, X. Wang, J. Li and L. Chen, *Talanta*, 2019, **195**, 390–400.
- 21 A. J. F. B. Jinhua Li and L. Chen, *Analyst*, 2018, **143**, 3570–3578.
- 22 X. Wu, X. Wang, W. Lu, X. Wang, J. Li, H. You, H. Xiong and L. Chen, *J. Chromatogr. A*, 2016, **1435**, 30–38.
- 23 H. Xiong, X. Wu, W. Lu, J. Fu, H. Peng, J. Li, X. Wang, H. Xiong and L. Chen, *Talanta*, 2018, **176**, 187–194.
- 24 A. Gruszkiewicz, M. Słowikowska, G. Grześ, A. Wójcik, J. Rokita, A. Fiocco, M. Wytrwal-Sarna, M. Marzec, B. Trzebicka, M. Kopeć, K. Wolski and S. Zapotoczny, *Eur. Polym. J.*, 2019, **112**, 817–821.
- 25 R. Dong, J. Li, H. Xiong, W. Lu, H. Peng and L. Chen, *Talanta*, 2014, **130**, 182–191.
- 26 A. X. W. A. Lingxin Chen, *Chem. Soc. Rev.*, 2016, **45**, 2137–2211.
- 27 C. Boutris, E. G. Chatzi and C. Kiparissides, *Polymer*, 1997, **38**, 2567–2570.
- 28 S. Çakmak, A. S. Çakmak and M. Gümüşderelioğlu, *Mater. Sci. Eng., C*, 2013, **33**, 3033–3040.
- 29 K. Nagase, T. Okano and H. Kanazawa, *Nano-Struct. Nano-Objects*, 2018, **16**, 9–23.
- 30 Q. Yu, Y. Zhang, H. Chen, Z. Wu, H. Huang and C. Cheng, *Colloids Surf., B*, 2010, **76**, 468–474.
- 31 S. Burkert, E. Bittrich, M. Kuntzsch, M. Müller, K. Eichhorn, C. Bellmann, P. Uhlmann and M. Stamm, *Langmuir*, 2010, **26**, 1786–1795.
- 32 J. Dong, J. Weng and L. Dai, *Carbon*, 2013, **52**, 326–336.
- 33 C. Chen, M. Liu, C. Gao, S. Lü, J. Chen, X. Yu, E. Ding, C. Yu, J. Guo and G. Cui, *Carbohydrate*, 2013, **92**, 621–628.
- 34 Y. Lin, H. Lin, J. Lin, B. Hsieh and Y. Sheng, *J. Colloid Interface Sci.*, 2012, **387**, 106–114.
- 35 M. Kohri, Y. Shinoda, H. Kohma, Y. Nannichi, M. Yamauchi, S. Yagai, T. Kojima, T. Taniguchi and K. Kishikawa, *Macromol. Rapid Commun.*, 2013, **34**, 1220–1224.
- 36 S. Hong, Y. S. Na, S. Choi, I. T. Song, W. Y. Kim and H. Lee, *Adv. Funct. Mater.*, 2012, **22**, 4711–4717.
- 37 X. Wang, G. Song and C. Deng, *Talanta*, 2015, **132**, 753–759.
- 38 Y. Song, X. Song, H. Yuan and C. Cheng, *New J. Chem.*, 2016, **40**, 3194–3207.
- 39 C. H. Hong, M. W. Kim, W. L. Zhang, I. J. Moon and H. J. Choi, *J. Colloid Interface Sci.*, 2016, **481**, 194–200.
- 40 B. Zhu and S. Edmondson, *Polymer*, 2011, **52**, 2141–2149.
- 41 T. P. Krishna Murthy, B. S. Gowrishankar, M. N. Chandra Prabha, M. Kruthi and R. Hari Krishna, *Microchem. J.*, 2019, **146**, 192–201.
- 42 Y. Yao, S. Miao, S. Liu, L. P. Ma, H. Sun and S. Wang, *Chem. Eng. J.*, 2012, **184**, 326–332.
- 43 M. Kohri, H. Kohma, Y. Shinoda, M. Yamauchi, S. Yagai, T. Kojima, T. Taniguchi and K. Kishikawa, *Polym. Chem.*, 2013, **4**, 2696.
- 44 Y. Yao, S. Miao, S. Liu, L. P. Ma, H. Sun and S. Wang, *Chem. Eng. J.*, 2012, **184**, 326–332.
- 45 P. Arabkhani and A. Asfaram, *J. Hazard. Mater.*, 2020, **384**, 121394.
- 46 S. A. R. Mirzajani, *J. Ind. Eng. Chem.*, 2015, **23**, 171–178.
- 47 Z. Lin, H. Zhang, L. Li and Z. Huang, *React. Funct. Polym.*, 2016, **98**, 24–30.
- 48 Z. Zhou, Y. Fu, Q. Qin, X. Lu, X. Shi, C. Zhao and G. Xu, *J. Chromatogr. A*, 2018, **1560**, 19–25.